LAWRENCE
LIVERMORE
NATIONAL
LABORATORY

LLNL-JRNL-664311

Reflective multilayer optic as X-ray diagnostic on laser-plasmaexperiment

N. F. Brejnholt, H. Chen, T. A. Decker, R. M. Hill, J. G. Williams, J. Peebles, M. A. Descalle

November 18, 2014

Review of Scientific Instruments

Disclaimer

Reflective multilayer optic as hard X-ray diagnostic on laser-plasma experiment

N. F. Brejnholt,[1, a)] T. A. Decker,[1] R. M. Hill,[1] H. Chen,[1] G. J. Williams,[1] J. Park,[1] J. B. Alameda,[1] M. Fernández-Perea,[1] M. J. Pivovaroff,[1] R. Soufli,[1] M.-A. Descalle,[1] J. Peebles,[2] and S. M. Kerr[3]

[1)] *Lawrence Livermore National Laboratory, Livermore, CA-94550, USA*

[2)] *Jacobs School of Engineering, UC San Diego, La Jolla, CA-92093, USA*

[3)] *University of Alberta, Alberta T6G 2R3, Canada*

(Dated: 26 February 2015)

A multilayer-based optic was tested for use as an X-ray diagnostic on a laser-plasma experiment. The multilayer optic was employed to selectively pass X-rays between 55-100 keV. An order of magnitude improvement in signal-to-noise ratio is achieved compared to a transmission crystal spectrometer. A multilayer response model, taking into account the source size and spectral content, is constructed and the outlook for application above 500 keV is briefly discussed. LLNL-JRNL-664311.

Keywords: Bragg reflector, multilayer, laser-plasma, hard X-ray

[a)]Electronic mail: brejnholt1@llnl.gov

I. INTRODUCTION

The development of hard X-ray (E>10 keV) photon diagnostics is important to both the research and eventual application of high-energy density (HED) plasmas on account of their ability to extract information from the plasma production site despite the high density of the system. Existing diagnostics generally operate in a transmission geometry, e.g. transmission crystal spectrometers[1] and Ross-filter pairs.[2] The former provides excellent spectral resolving power, but has low throughput, while the latter allows higher throughput with limited resolving power. In this paper we demonstrate an alternative approach utilizing multilayer optics, which operate in reflection geometry. The reflection geometry allows a significantly higher throughput to be achieved, while retaining good spectral resolving capabilities over a tunable energy range. These features are very valuable for a number of HED studies where signal collection efficiency is important. Examples include intense laser-plasma interactions[3], high-energy backlighter development for inertial confinement fusion[4], Compton radiography[5] and gamma emissions from nuclear processes.[6]

Hard X-ray multilayer optics have seen increasing use over the last few decades as deposition and characterization techniques have improved and the scientific user base grown, particularly driven by the synchrotron and astrophysics communities, and recently by nuclear safeguards applications.[7] At synchrotron light sources, multilayer coatings are enabling components of ultra-high resolution gratings for spectrometry, and can achieve nano-focusing when used in either diffractive (multilayer Laue lenses) or reflective geometries.[8] Multilayers also recently enabled the first space-borne focusing optics above 10 keV, carried on-board the NASA NuSTAR satellite,[9] providing important new insights into the evolution of our Universe.[10–12] Within the last few years multilayer mirrors reflectivity has been shown to be efficient and well-understood up to 645 keV[13**?**] demonstrating that focusing multilayer optics operating close to the MeV range are feasible.

Based on these developments, we deployed a multilayer optic as a novel diagnostic for a laser-plasma interaction experiment at the Jupiter Laser Facility (JLF) at Lawrence Livermore National Laboratory, selectively passing X-rays in the 55-100 keV photon energy range. The data is shown to match predictions based on a simple multilayer response model and the potential for use at higher energies is discussed.

II. MULTILAYER OPTICS

A multilayer optic relies on constructive interference in the multilayer structure to efficiently reflect radiation at grazing incidence angles greater than the critical angle. In the X-ray energy regime the critical angle describes the angle below which total external reflection occurs.[14,15] The multilayer structure is typically made up of N number of bilayers, each bilayer consisting of a layer of high-Z (absorber) and a layer of low-Z (spacer) materials as illustrated in Fig. 1. The electron-density contrast between the absorber and the spacer governs the efficiency of the constructive interference. The theoretical efficiency can be significantly degraded by imperfections in the interfaces between individual layers, i.e. interdiffusion and roughness. For the present work, the Fresnel equations including Névot-Croce factors[16] are used to calculate the multilayer response, but for an intuitive understanding of multilayers, the allowed reflections can be approximated using Bragg's law

$$n\lambda = 2dsin(\theta_B) \tag{1}$$

From Eq. (1), radiation of wavelength λ is specularly reflected by a multilayer with bilayer period thickness d when impinging at a grazing incidence angle θ_B. Only the first order reflection ($n = 1$) is relevant to this work as higher order reflections have $> 10^3$ times lower efficiency. Coupled with fewer short wavelength photons and lower detector sensitivity the higher order signal is many orders of magnitude below background.

One of the major strengths of the multilayer is that the design can be tailored to the intended application. For a narrow band-pass filter a single period d is used for all N bilayers (Fig. 1), while a broad passband can be achieved by depth-grading d during multilayer deposition, i.e. creating overlapping Bragg reflections. The latter was used to achieve high broadband efficiency for the NuSTAR optics.[17] Multilayers can furthermore be designed to increase throughput in multiple specific bands or to compensate for undesirable experimental artifacts, such as beam divergence.

A tungsten carbide (WC)/silicon carbide (SiC) multilayer mirror with $N = 300$ and nominal period thickness $d = 15.2$ Å was used for this work. The WC/SiC multilayer coating was deposited by DC-magnetron sputtering on a 150x150 mm^2 super-polished fused silica substrate. The mirror has been extensively characterized using 0.8-8 keV X-rays and its response has been measured at photon energies up to 645 keV.[13? ?]

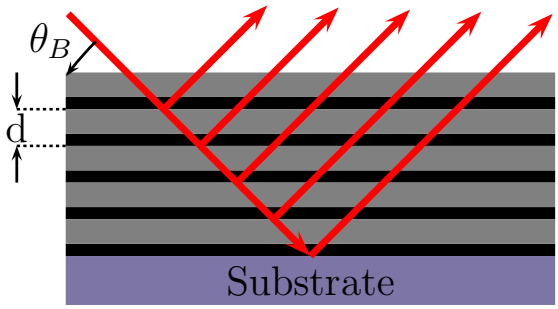

FIG. 1. A $N = 5$ multilayer with period d. Incident radiation (red) is reflected according to Bragg's law (Eq. (1)) for a given grazing incidence angle θ_B.

For the photon energy range investigated in this work the intrinsic bandpass of the multilayer is <1% (FWHM). Factors associated with the experiment, such as source parameters (size and intensity profile) and the geometry of the setup (mirror length, collimators and distance between components) will in most cases broaden the passed band beyond the intrinsic value. The parameters relating to the setup and the mirror are known for the experiment and as a result the modeling will be sensitive to the source size, intensity and spectral content. In this work, a line source with spatially uniform intensity and energy distribution is assumed. A more complex source would act to weigh contributions from different sections of the mirror. The impact on the response is a second order effect. The photon spectra used as input in our model were simulated with the Geant4 Monte Carlo code[18] assuming a Maxwellian input electron distribution with $T_{hot} = 6.0$ MeV incident on the target.

Fig. 2 shows the predicted response of the multilayer mirror for a gold (Au) target in the experimental setup described in the next section. The output for both a 200 and 500 μm line source is shown to demonstrate the sensitivity to source size. The broadening of the characteristic X-ray lines is apparent, as is the suppression of the out-of-band response. The response is calculated using custom-written software and the software package IMD[16]. The software takes the beam divergence and source size into account, and assumes the mirror is at a nominal angle θ_B given by Eq. (1). The nominal angle is tuned to match the X-ray energy ($E = hc/\lambda$) of interest during the experiment.

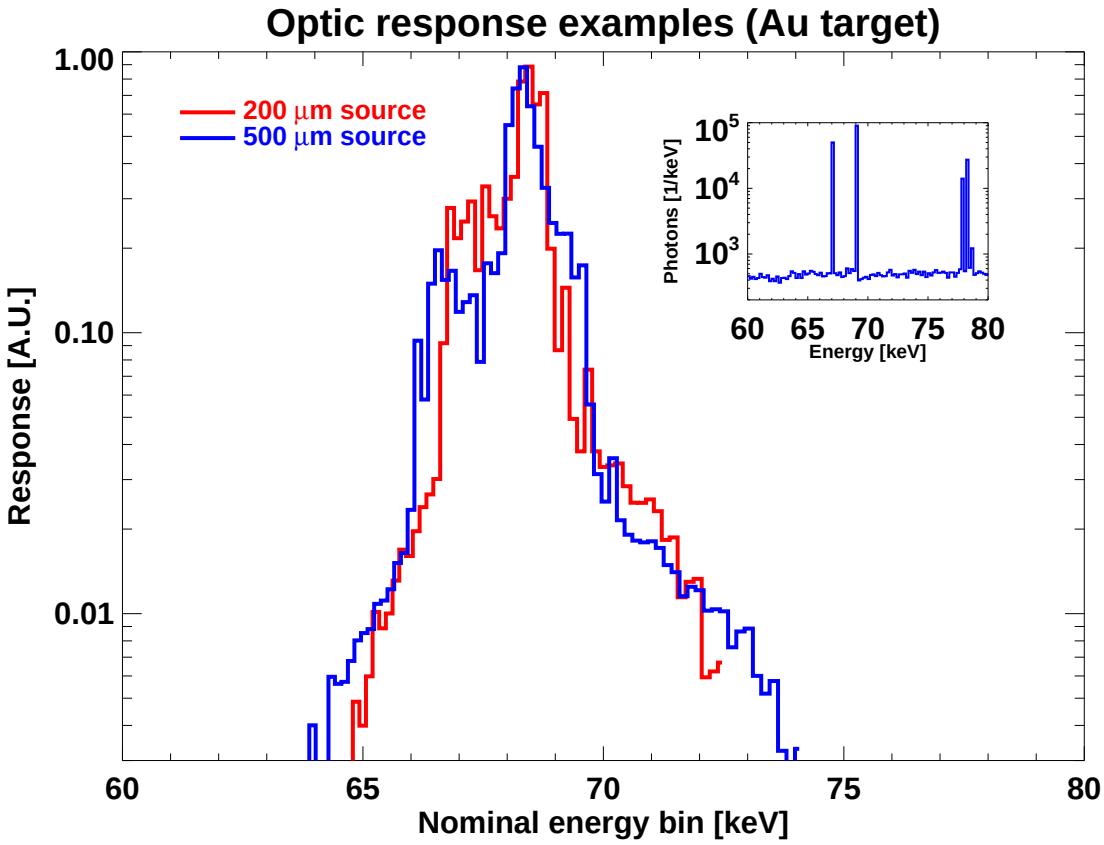

FIG. 2. Predicted response with the optic aligned to favor Au-K_{α_1} ($E = 68.806$ keV). The simulated input spectrum is shown in inset.

III. EXPERIMENT

This experiment was conducted at the JLF using the Titan short pulse laser system. A 1054 nm, 10 ps laser pulse with laser energy 250-280 J at the target was used. The laser pulse interacts with the front target surface plasma accelerating electrons to relativistic energies of several MeV.[19] The electrons in turn generate characteristic X-rays and bremsstrahlung as they stream through the target material. The laser was focused to 15 μm FWHM, measured in vacuum at low intensity, by an $f/3$ parabolic mirror. Thick (0.5-1.0 mm), high-Z targets of tantalum ($Z_{Ta} = 73$), tungsten ($Z_W = 74$), gold ($Z_{Au} = 79$), and uranium ($Z_U = 92$) were irradiated with a laser intensity of roughly 1.6×10^{19} W/cm^2.

The experimental setup is outlined in Fig. 3. The multilayer mirror was situated immediately outside the Titan vacuum chamber. A 1 mm wide mirror collimator limits the incident radiation to a maximum beam divergence of 0.08°, essentially acting as a high-pass photon

energy filter, preventing very divergent, low-energy photons from being reflected. The finite length of the mirror and size of the source result in the mirror's photon energy band-pass increasing to about 6% at 60 keV and 10% at 100 keV.

The mirror angle relative to the line of sight (LoS) between the detection plane and the target chamber center (TCC), where the target is installed, was monitored and kept within 20" of the desired value throughout the experiment using a high-precision digital auto-collimator. This angle corresponds to θ_B in Eq. (1) and was adjusted prior to each shot so that the mirror's photon energy bandpass was centered at the K_{α_1} line for the relevant target material. The broadened photon energy bandpass is sufficient to pass the entire K_α line complex.

In the detection plane, Fujifilm BSA-MS image plates were mounted in a lead (Pb) enclosure. The image plates were read out by a calibrated Fuji-FLA-7000 scanner.[20]

Pb collimators were installed between the multilayer mirror and the image plate detector to reduce background originating from the laser-induced high energy (>MeV) radiation. In addition to collimators, several in-line filters were installed between TCC and the image plate, including a 1.0 T magnet to sweep away energetic electrons emitted from the target inside the vacuum chamber, a 500 μm thick Be window on the chamber and a 3 mm Al plate. Low energy photons were further attenuated by close to four meters of air separating the source from the detector. The filters are essential to keep background low in the detection plane and to filter out photons undergoing total external reflection.

To relate results from the new diagnostic to established laser-plasma diagnostic tools a crystal spectrometer was also deployed, as shown in Fig. 3. The Laue transmission crystal spectrometer,[1] or Gamma Crystal Spectrometer (GCS) uses a 400 μm thick, cylindrically bent germanium (220) crystal with a radius of curvature of 965 mm covering the X-ray energy range 50-300 keV. The GCS was positioned inside the target chamber at a glancing angle of 3°. X-rays diffracted by the crystal passed through a 2.5 cm tungsten crossover slit and 1.5 mm of aluminum filtering before reaching the image plate detector.

IV. RESULTS AND DISCUSSION

Images from four laser shots are shown in Fig. 4. Line structures are apparent in each image, confirming that the mirror selectively reflects both K_{α_1} and K_{α_2}. The K_{α_3} line does

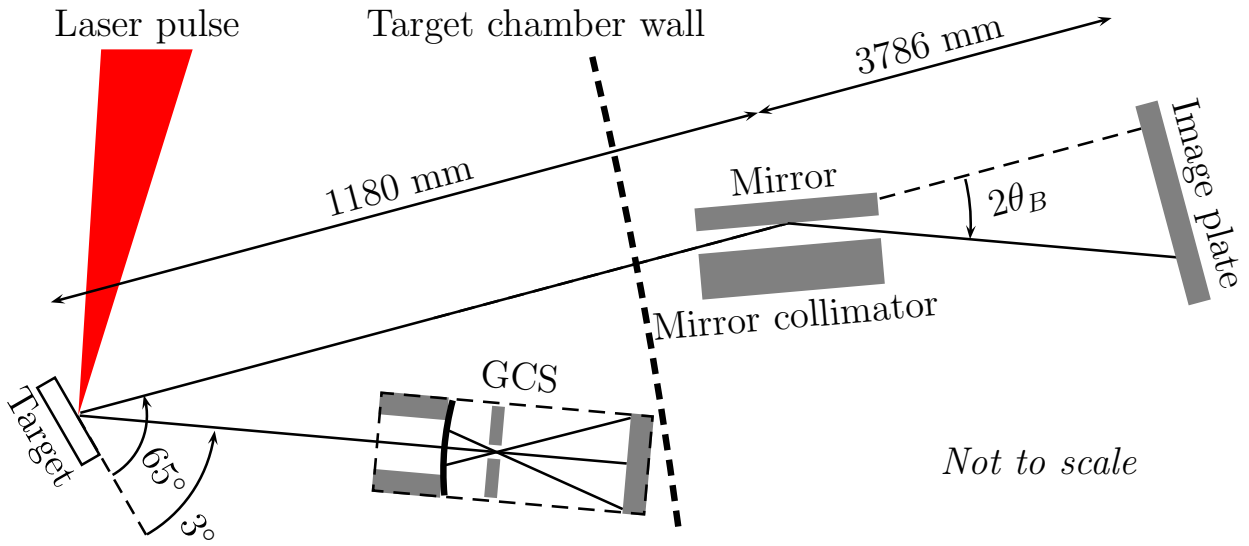

FIG. 3. Outline of multilayer mirror and GCS setup for Titan experiment. High-energy collimators and low-energy inline filters are not shown.

not feature prominently on account of its much lower relative intensity. The line structures are more readily observed when collapsing the data to line plots, as shown in Fig. 5. The figure includes data from the GCS diagnostic for comparison. The best GCS data acquired in this campaign were selected for the comparison. Although U-K_α lines were not observed with the GCS, a data set is plotted for completeness. The multilayer data indicates a weaker U line complex, confirming that the characteristic X-ray production from U dropped below the detection limit of the GCS. In general the multilayer response is more than an order of magnitude above background, whereas the best GCS data is at most two times higher. Previously reported GCS studies achieved signal-to-noise ratios up to five at 43 keV.[21]

The line plots show the data sorted into nominal energy bins whose value is derived for each horizontal pixel (Fig. 4) using Eq. (1) and assuming a nominal multilayer period. θ_B is found from the displacement between LoS and the pixel in question.

While Fig. 4 and Fig. 5 demonstrate the capability of the multilayer optic to selectively reflect part of the incident photon spectrum, the displayed data does not immediately provide information about the source. To achieve this the model demonstrated in Fig. 2 is used again. The IMD software outputs the reflectivity of the mirror as a function of angle and energy and the custom IDL software propagates the output to the detector plane where it is re-binned to nominal energy bins. The result is shown in Fig. 6. A line source with uniform spectral

content and intensity was assumed using simulated spectra (Fig. 6 insets). The length of the line source was adjusted for best fit, and the estimated source size was found to vary from 350 to 400 μm depending on the target material. The estimated size matches previous findings.[22]

It is worth noting that the experimental setup used can also reflect photons at higher energies. However, estimates indicated that low photon flux and image plate sensitivity above 200 keV would prevent the reflected signal from being observable above the readout noise of the scanner. This was confirmed with several trial shots with the mirror aligned to reflect 200 and 511 keV photons. Several orders of magnitude improvement in signal-to-noise ratio is advisable for such measurements, e.g. through greater collection area (nested multilayer optic), a detector with higher sensitivity or increased photon flux. When moving to these extreme grazing incidence angles, it is important to keep in mind that total external reflection will become an increasingly important noise component. As an example, the critical angle at which Au-K_{α_1} undergoes total external reflection is approximately 0.042°, which is comparable to the grazing incidence angle for 511 keV photons (refer to Eq. (1)) in this experiment. Coupled with the image plate's higher sensitivity to lower energies and the increased intensity of the K_α signal significant filtering is necessary. For the 511 keV trial shots carried out here a 0.5 mm Ta filter was used, attenuating < 100 keV photons by more than 98% at a cost of 10% of the 511 keV signal.

V. SUMMARY

An X-ray photon diagnostic based on reflective multilayer optic technology was tested during a laser-plasma experiment conducted at the JLF. The K_α line complexes of four high-Z materials (Ta, W, Au and U) were preferentially reflected and successfully detected. Comparisons to data acquired with a transmission crystal spectrometer showed an order of magnitude improvement in signal-to-noise ratio for the multilayer optic. The improved efficiency enabled detection of the U-K_α line complex, demonstrating how a multilayer-based optic may supplement or replace existing diagnostics in photon-starved experiments where good spectral resolving capabilities are required. The multilayer data was successfully modeled showing that the technique can provide detailed information about the source.

This successful proof-of-concept test, combined with other work having demonstrated

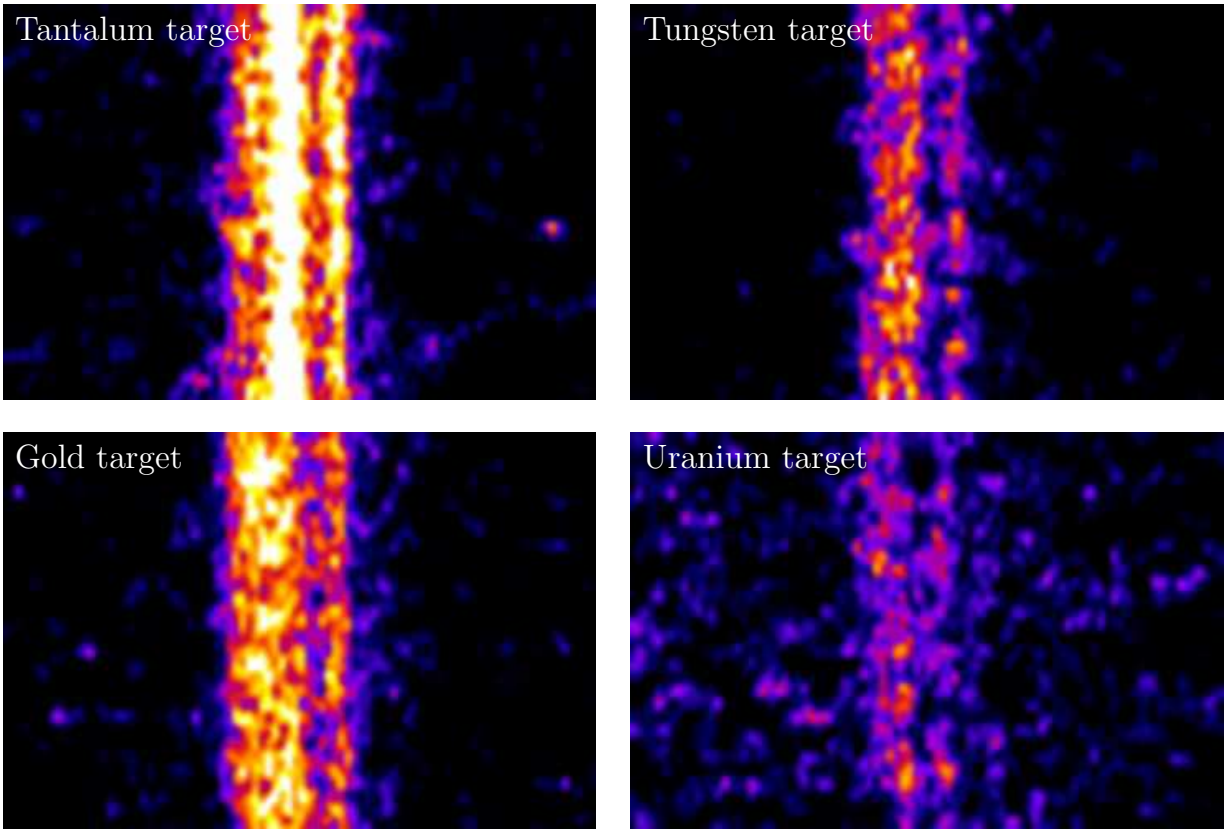

FIG. 4. 60x90 pixel^2 sub-selections of the image plate readout showing the reflected beam for each of the four target materials. The pixel size for image plate scans was set to 100 μm.

that the multilayer optic technology is applicable up to at least 645 keV, sets the stage for attempting to detect the 511 keV electron-positron annihilation line. Challenges associated with this task include finding a suitable detector and increasing the collection area, e.g. through the design and construction of a more complex, nested multilayer optic.

VI. ACKNOWLEDGEMENTS

This work performed under the auspices of the U.S. Department of Energy by Lawrence Livermore National Laboratory under Contract DE-AC52-07NA27344. Funding was provided by the Livermore Graduate Scholar Program and LLNLs Laboratory Directed Research and Development Program through project 13-ERD-048 and 12-ERD-062. The authors gratefully acknowledge support from the staff at the Jupiter Laser Facility and valuable input from Gary F. Stone.

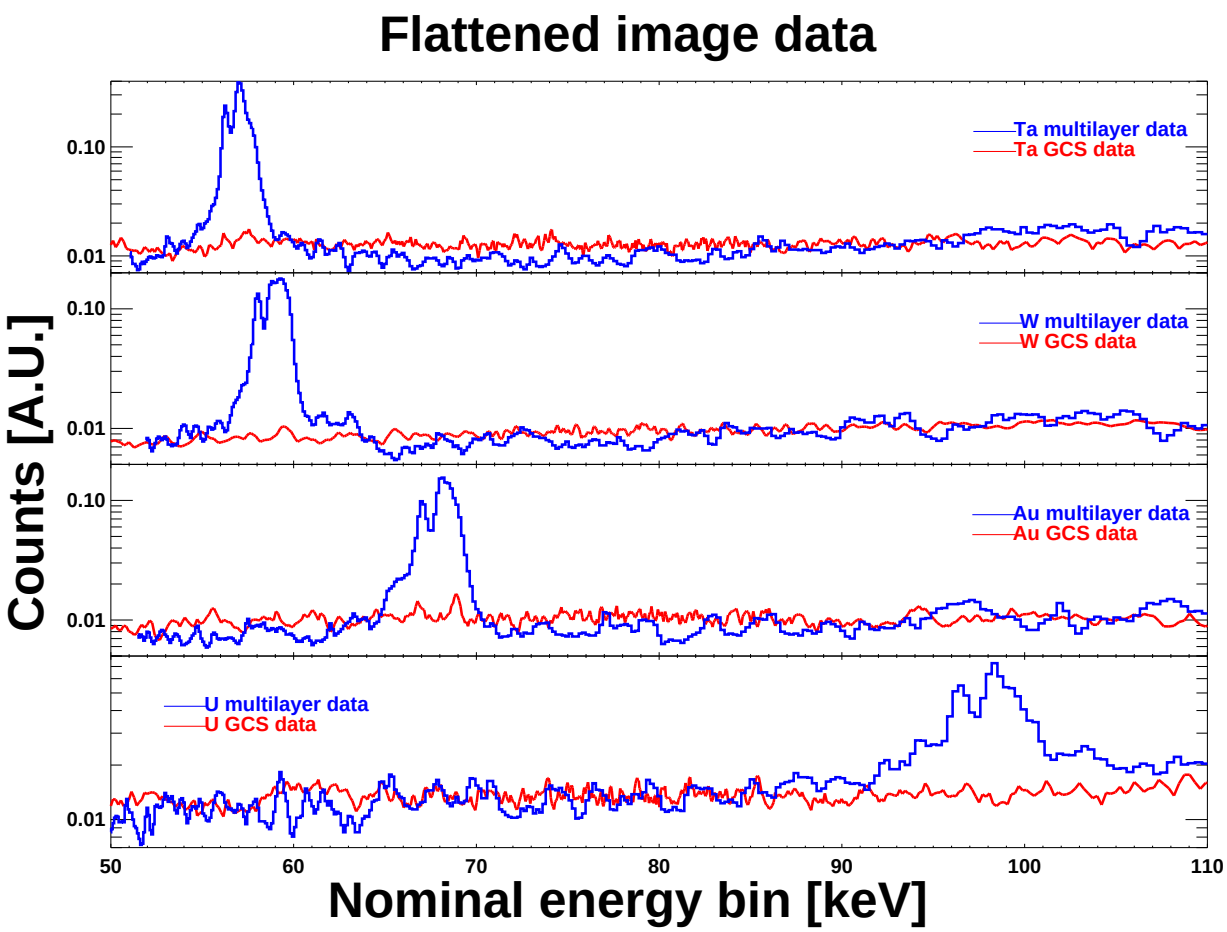

FIG. 5. Flattened image data from the multilayer and GCS diagnostic tools. Fig. 4 images were flattened to line plots by summing 50 vertical pixels. The GCS data were summed over 200 vertical pixels (pixel size 50 μm).

REFERENCES

[1]J. F. Seely, L. T. Hudson, G. E. Holland, and A. Henins, Appl. Opt. **47**, 2767 (2008).

[2]P. A. Ross, Journal of the Optical Society of America **16**, 433 (1928).

[3]S. P. D. Mangles, C. D. Murphy, Z. Najmudin, A. G. R. Thomas, J. L. Collier, A. E. Dangor, E. J. Divall, P. S. Foster, J. G. Gallacher, C. J. Hooker, and et al., Nature **431**, 535 (2004).

[4]H.-S. Park, B. R. Maddox, E. Giraldez, S. P. Hatchett, L. T. Hudson, N. Izumi, M. H. Key, S. Le Pape, A. J. MacKinnon, A. G. MacPhee, and et al., Phys. Plasmas **15**, 072705 (2008).

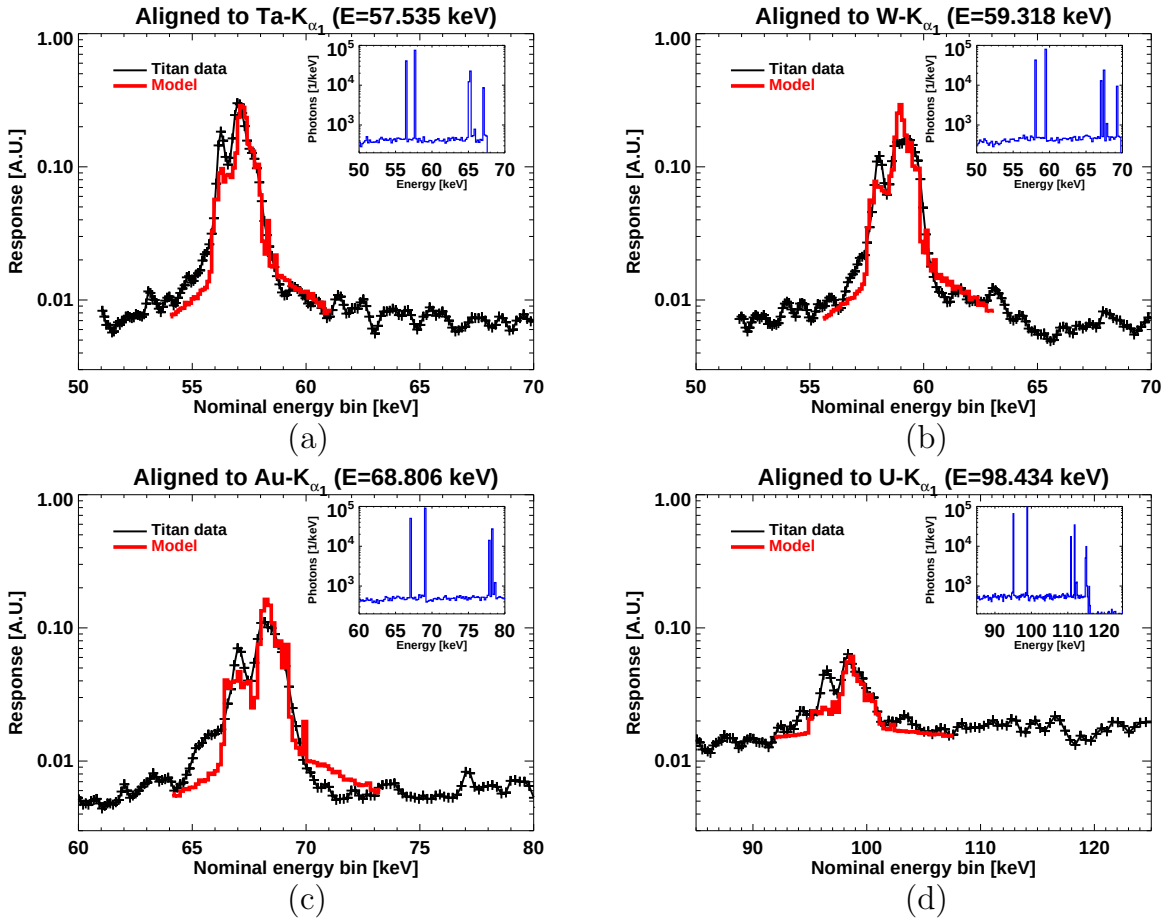

FIG. 6. Model and data for the four targets. Best fit was found by adjusting source size. Simulated input spectra used are shown in insets (a) 400 μm Ta line source (b) 400 μm W line source (c) 350 μm Au line source (d) 350 μm U line source

[5]R. Tommasini, S. P. Hatchett, D. S. Hey, C. Iglesias, N. Izumi, J. A. Koch, O. L. Landen, A. J. MacKinnon, C. Sorce, J. A. Delettrez, and et al., Phys. Plasmas **18**, 056309 (2011).

[6]G. Shvets, Nat Phys **7**, 834 (2011).

[7]M. J. Pivovaroff, K. P. Ziock, M. Fernandez-Perea, M. J. Harrison, and R. Soufli, Nucl. Instrum. Meth. A **743**, 109 (2014).

[8]D. Miller and H. Padmore, "X-ray optics for bes light source facilities," Tech. Rep. (U.S. Department of Energy, 2013).

[9]F. A. Harrison, W. W. Craig, F. E. Christensen, C. J. Hailey, W. W. Zhang, S. E. Boggs, D. Stern, W. R. Cook, K. Forster, P. Giommi, and N. F. Brejnholt, Astrophys. J. **770**, 103 (2013).

[10]B. W. Grefenstette, F. A. Harrison, S. E. Boggs, S. P. Reynolds, C. L. Fryer, K. K. Madsen, D. R. Wik, A. Zoglauer, C. I. Ellinger, and D. M. Alexander, Nature **506**, 339 (2014).

[11]G. Risaliti, F. A. Harrison, K. K. Madsen, D. J. Walton, S. E. Boggs, F. E. Christensen, W. W. Craig, B. W. Grefenstette, C. J. Hailey, and E. Nardini, Nature **494**, 449 (2013).

[12]M. Bachetti, F. A. Harrison, D. J. Walton, B. W. Grefenstette, D. Chakrabarty, F. Fuerst, D. Barret, A. Beloborodov, S. E. Boggs, F. E. Christensen, and et al., Nature **514**, 202 (2014).

[13]N. F. Brejnholt, M. Descalle, R. Soufli, M. J. Pivovaroff, and F. Christensen, Optics Express **13**, 15364 (2014).

[14]E. Spiller *et al.*, *Soft X-ray optics* (SPIE Press, 1994).

[15]D. Attwood, *Soft X-rays and Extreme Ultraviolet Radiation* (Cambridge University Press, 1999).

[16]D. L. Windt, Comput. Phys. **12**, 360 (1998).

[17]F. E. Christensen, A. C. Jakobsen, N. F. Brejnholt, K. K. Madsen, A. Hornstrup, N. J. Westergaard, J. Momberg, J. Koglin, A. M. Fabricant, M. Stern, and et al., Optics for EUV, X-Ray, and Gamma-Ray Astronomy V (2011), 10.1117/12.894615.

[18]S. Agostinelli, J. Allison, K. Amako, J. Apostolakis, H. Araujo, P. Arce, M. Asai, D. Axen, S. Banerjee, G. Barrand, and et al., Nuclear Instruments and Methods in Physics Research Section A: Accelerators, Spectrometers, Detectors and Associated Equipment **506**, 250 (2003).

[19]S. Wilks, W. Kruer, M. Tabak, and A. Langdon, Physical Review Letters **69**, 1383 (1992).

[20]G. J. Williams, B. R. Maddox, H. Chen, S. Kojima, and M. Millecchia, Review of Scientific Instruments **85**, 11E604 (2014).

[21]J. F. Seely, C. I. Szabo, P. Audebert, E. Brambrink, E. Tabakhoff, and L. T. Hudson, Phys. Plasmas **17**, 023102 (2010).

[22]H. Chen, J. C. Sheppard, D. D. Meyerhofer, A. Hazi, A. Link, S. Anderson, H. A. Baldis, R. Fedosejev, J. Gronberg, N. Izumi, and et al., Phys. Plasmas **20**, 013111 (2013).